lubricants

MDPI

Article

Comprehensive Investigation into the Effects of Structural Factors on the Shear Stability of High-Viscosity Metallocene Poly(α-Olefins)

Jingchun Zhang [1], Jian Xu [1], Zhongxiang Bai [2], Xuemei Liang [2], Ruilong Li [2], Jianxin Shi [2,*] and Jiusheng Li [1,*]

[1] Laboratory for Advanced Lubricating Materials, Shanghai Advanced Research Institute, Chinese Academy of Sciences, Shanghai 201210, China; zhangjingchun@sari.ac.cn (J.Z.); xujian@sari.ac.cn (J.X.)
[2] Ningxia Coal Industry Co., Ltd., CHN Energy, Yinchuan 750411, China; 15111127@ceic.com (Z.B.); 15103756@ceic.com (X.L.); 15010217@ceic.com (R.L.)
* Correspondence: 12026895@ceic.com (J.S.); lijs@sari.ac.cn (J.L.)

Abstract

High-viscosity metallocene poly(α-olefins) are important synthetic lubricant base oils. However, the effects of molecular structure on permanent viscosity loss during mechanical shearing remain insufficiently understood. In this study, mPAO with varying monomer carbon numbers, kinematic viscosities, molecular weight distributions, chain stereoregularities, and residual unsaturation levels were investigated using KRL shear testing, gel permeation chromatography, and spectroscopic characterization. The results showed that the number-average molecular weight decreased and the molecular weight distribution broadened after shearing, whereas the weight-average molecular weight changed only slightly, suggesting that molecular weight changes primarily involved a fraction of the polymer chains. Fourier transform infrared spectroscopy revealed oxidation-related changes after shearing, suggesting that oxidation-induced viscosity increase may partially offset shear-induced viscosity loss. Different side-chain structures exhibited distinct shear responses as the monomer carbon number varied. For samples with similar side-chain structures, the viscosity loss rate increased nonlinearly and in a stepwise manner with increasing backbone length. A broader initial molecular weight distribution was associated with greater PVL, whereas higher chain stereoregularity and lower residual unsaturation were associated with improved shear stability. These findings clarify the relationships between molecular structural parameters and the mechanical shear stability of mPAO, providing a basis for designing high-viscosity lubricant base oils with improved shear stability.

Keywords: mPAO; shear stability; viscosity loss; molecular structure regulation; structure–property relationship

Received: 30 October 2026
Revised: 10 November 2026
Accepted: 12 November 2026
Published: 16 November 2026

Copyright: © 2026 by the authors. Licensee MDPI, Basel, Switzerland. This article is an open access article distributed under the terms and conditions of the Creative Commons Attribution (CC BY) license.

1. Introduction

With the rapid global transition toward renewable energy, wind power has become an indispensable component of modern power systems [1,2]. As the core component of wind turbine transmission systems, wind turbine gearboxes are frequently subjected to severe impact loads and high-frequency torque fluctuations during operation. The internal gears and bearings continuously experience intense contact stresses and cyclic shear forces [3–6].

Under the coupled effects of continuous mechanical shear, frictional heat generation, and exposure to the air environment, macromolecules in lubricating oils undergo irreversible chemical chain scission. This process leads to permanent viscosity loss, resulting in reduced lubricant film thickness, decreased oxidation resistance and load-bearing capacity, and ultimately affecting the operational reliability and service life of gearboxes [7,8].

With the development of wind turbines toward larger scale, higher power output, and longer service life, higher requirements have been imposed on the viscosity–temperature performance, oxidation stability, and shear resistance of lubricant base oils used in wind turbine gearboxes [9,10]. Therefore, the development of base oils with excellent rheological properties and high shear stability has become an important direction for advanced wind turbine gear oils [11]. In recent years, mPAO products have attracted increasing attention due to their unique molecular structures and excellent comprehensive properties [12]. Benefiting from the precise control of polymerization reactions enabled by metallocene-catalyzed polymerization technology, mPAO products generally exhibit narrower molecular weight distributions, higher structural uniformity, and tunable branched-chain topologies [13]. Compared with conventional PAO, mPAO products possess higher viscosity indices, superior low-temperature flow properties, and lower volatility losses. Therefore, they have gradually become important base oils or blending components for advanced wind turbine gear oils and show promising application potential in long-life industrial lubrication systems.

Currently, research on the shear resistance of lubricating oils mainly focuses on polymer viscosity index improver systems. Previous studies have investigated the effects of comb-like, star-shaped, dendritic, and crosslinked polymer structures on the viscosity index, shear stability, and rheological properties of lubricating oils, providing important guidance for the development of high-performance lubricant formulations [14–17]. However, these studies usually introduce polymers as functional additives into base oils or directly evaluate commercial lubricant formulations. The obtained results therefore represent the combined effects of base oils, polymers, and other additives, making it difficult to distinguish the intrinsic contribution of base oil molecular structures to shear resistance. Meanwhile, a limited number of experimental and molecular simulation studies on base oils have demonstrated that the molecular structure of base oils can significantly influence lubrication behavior. Different branching configurations, topological structures, and molecular compositions can affect oil film formation, interfacial adsorption, friction characteristics, and load-bearing capacity [18–20]. These studies clearly indicate that the molecular structure of base oils itself is an important factor determining lubrication performance. They also highlight the scientific importance of establishing structure–property relationships of base oils for the design of high-performance lubricating materials. However, existing studies on base oils have mainly focused on tribological properties, interfacial interactions, and rheological behaviors [21,22]. In contrast, few studies have investigated the permanent viscosity loss of base oils under continuous mechanical shear. For high-viscosity mPAO base oils, the relationship between molecular structure and permanent viscosity loss is still not well understood. It remains unclear how different structural parameters affect the mechanical shear stability of mPAO and whether their effects vary. In contrast, few studies have investigated the permanent viscosity loss of base oils under continuous mechanical shear. For medium- and high-viscosity mPAO base oils, the relationship between molecular structure and permanent viscosity loss is still not well understood. It remains unclear how different structural parameters affect the mechanical shear stability of mPAO and whether their effects vary.

To address this issue, this study focuses on high-viscosity mPAO 300 base oils. Five key parameters are investigated: the carbon number of the α-olefin feedstock, kinematic viscosity, molecular weight distribution, stereoregularity, and unsaturated bond content.

https://doi.org/10.3390/lubricants14110436

Their effects on the intrinsic mechanical shear stability of the base oils are studied. Accelerated shear degradation tests are carried out using the standard KRL tapered roller bearing test under controlled cyclic mechanical loading in elastohydrodynamic lubrication conditions. The permanent viscosity loss of samples with different structural parameters is then compared to examine how these parameters affect mechanical shear stability. This study aims to establish the relationship between the molecular structure of mPAO base oils and their permanent viscosity loss. The results may help explain how molecular structure affects the mechanical shear stability of mPAO and provide a basis for designing and developing lubricant base oils with high shear stability.

2. Materials and Methods

2.1. Materials

1-Hexene, 1-octene, 1-decene, 1-dodecene, toluene, triisobutylaluminum, acidic clay, N,N-dimethylanilinium tetrakis(pentafluorophenyl)borate, and diatomaceous earth were purchased from Tansoole (Titan Scientific Co., Ltd., Shanghai, China).

2.2. Synthesis

First, 300 g of 1-hexene was added to a dry four-neck flask. Before the reaction, the system was purged three times with high-purity nitrogen to remove moisture and oxygen. Meanwhile, a catalyst solution was prepared in a dry Schlenk flask by dissolving rac-Et(Ind)$_2$ZrCl$_2$ (0.012 g) in toluene (10 mL), followed by the sequential addition of N,N-dimethylanilinium tetrakis(pentafluorophenyl)borate ([PhN(Me)$_2$H] B(C$_6$F$_5$)$_4$, 0.024 g) and triisobutylaluminum (TIBA, 2 mL). The resulting mixture was vigorously shaken for 1 min to activate the metallocene catalyst system. After 1-hexene was heated to 95 °C, the pre-activated catalyst solution was added to the reaction system in five portions. The polymerization reaction was continuously stirred at 95-105 °C. After completion of the polymerization, acidic clay and diatomaceous earth were added to the reaction system to adsorb residual catalysts and polar impurities. After further stirring for 1 h, the mixture was filtered to obtain the crude mPAO product. The obtained crude product was subjected to vacuum distillation using a thin-film evaporator at 245 °C and 1.2 mbar to remove unreacted monomers, oligomeric by-products, and light components, yielding the unrefined mPAO base oil. Subsequently, the obtained mPAO base oil was hydrogenated in a high-pressure hydrogenation reactor under 30 bar hydrogen pressure at 225°C. A hydrogenation catalyst was added at a dosage of 0.5 g per 100 g of base oil, and the reaction was conducted for 5 h. After filtration to remove the hydrogenation catalyst, the final mPAO product was obtained. Using the same procedure, homopolymerized mPAO base oils prepared from 1-octene, 1-decene, and 1-dodecene were synthesized. In addition, copolymerized mPAO base oils were prepared using 1-hexene/1-octene, 1-octene/1-decene, and 1-decene/1-dodecene feedstocks with a molar ratio of 1:1. According to the average carbon number of the monomers in the obtained mPAO, the samples were denoted as C$_6$, C$_7$, C$_8$, C$_9$, C$_{10}$, C$_{11}$, and C$_{12}$.

Different viscosity grades of mPAO base oils were synthesized by adjusting the polymerization temperature. All samples were prepared using 1-octene as the feedstock, while the other reaction conditions were kept unchanged. The obtained samples were denoted as mPAO150, mPAO200, mPAO250, mPAO300, mPAO350, and mPAO400.

mPAO samples with different molecular weight distributions were prepared by adjusting the control range of the polymerization temperature. All samples were synthesized using 1-octene as the feedstock, and the other reaction conditions were maintained constant. The samples were denoted as mPAO-D1, mPAO-D2, mPAO-D3, and mPAO-D4.

mPAO samples with different stereoregularities were synthesized by adjusting the type of metallocene catalyst. All samples were prepared using 1-decene as the feedstock, while the other reaction conditions remained unchanged. The sample prepared using rac-$Me_2Si(ind)_2ZrCl_2$ was denoted as mPAOI1; the sample prepared using rac-Me_2Si(4,7-dimethyl-ind)$_2ZrCl_2$ was denoted as mPAOI2; the sample prepared using rac-$Et(Ind)_2ZrCl_2$ was denoted as mPAOI3; and the sample prepared using meso-$Et(Ind)_2ZrCl_2$ was denoted as mPAOI4.

mPAO samples with different unsaturated double-bond contents were obtained by adjusting the hydrogenation temperature. All samples were prepared using 1-octene as the feedstock, and the other reaction conditions were kept constant. The samples were denoted as mPAO-H1, mPAO-H2, mPAO-H3, and mPAO-H4.

The synthesis of the metallocene catalyst is described in detail in the Supplementary Information.

2.3. KRL Shear Test

To investigate the structural stability and viscosity degradation behavior of mPAO 300 base oil under long-term mechanical shear, mechanical shear tests were performed using a tapered roller bearing shear stability test with reference to the CEC L-45-A-99 standard. The experiments were conducted using a VKA110 (Hansa Press- und Maschinenbau GmbH, Hamburg, Germany) tapered roller bearing shear stability testing apparatus manufactured by Hansa, Germany. Before the tests, the tapered roller bearings and related components were cleaned with petroleum ether and ethanol, followed by drying with compressed air. Subsequently, 40.0 mL of the test oil sample was added to the test chamber. The assembled tapered roller bearing components were then installed in the testing apparatus, and a load of 5000 N was applied. During the test, the temperature was maintained at 60 °C. Under constant temperature conditions, the bearing was operated at a rotational speed of 1475 rpm and subjected to continuous shear for 1,770,000 revolutions, corresponding to a test duration of approximately 20 h. After completion of the test, the sheared oil samples were collected for subsequent viscosity measurements and molecular structural characterization. The viscosities mentioned in this study refer to the values measured at 100 °C. The viscosity data of mPAO before and after shearing are provided in the Supplementary Information.

2.4. Characterization

Fourier transform infrared (FT-IR) spectroscopy (Frontier, PerkinElmer, Shelton, CT, USA) was used to analyze the samples before and after shear testing. The spectra were recorded over a wavenumber range of 4000–400 cm^{-1}. The measurements were performed using a liquid cell transmission mode, and the background was corrected using air as the reference. Nuclear magnetic resonance (NMR) measurements were conducted using an ADVANCE Ⅲ HD spectrometer (Bruker, Billerica, MA, USA). A certain amount of sample was dissolved in $CDCl_3$, with tetramethylsilane (TMS) used as the internal chemical shift reference. The corresponding ^1H NMR and ^{13}C NMR spectra were collected. The molecular weight and molecular weight distribution of the samples were determined using a gel permeation chromatography (GPC) system (1260 Infinity II GPC/SEC System, Agilent Technologies, Santa Clara, CA, USA). Tetrahydrofuran was used as the mobile phase at a flow rate of 1.0 $mL \cdot min^{-1}$. Detailed GPC test data are provided in the Supplementary Information.

3. Results

3.1. α-Olefin Feedstock Carbon Number

Figure 1a shows the viscosity variation behavior of mPAO samples prepared from α-olefin feedstocks with different carbon numbers after KRL standard mechanical shear testing. Under mechanical shear, lubricant molecular chains undergo continuous stretching and scission, resulting in a decrease in base oil viscosity. Therefore, the viscosity reduction rate after shear can be used as an important indicator for evaluating the molecular structural stability and mechanical shear resistance of mPAO. It can be observed that the carbon number of the polymerization feedstock has a significant effect on the mechanical shear stability of mPAO. However, this effect does not show a monotonic variation with increasing carbon number. The C6, C8, C10, and C12 samples prepared from pure α-olefin monomers exhibited excellent shear stability, with viscosity reduction rates of −0.34%, 1.76%, 3.12%, and 2.15%, respectively. In contrast, the C7, C9, and C11 samples obtained by copolymerization of α-olefins with different carbon numbers showed more pronounced viscosity changes compared with the corresponding homopolymers. Among them, the C9 sample exhibited the highest viscosity reduction rate of 6.31%. The viscosity reduction rate of the C11 sample was 3.92%, while the C7 sample also showed a more significant viscosity increase than the C6 sample. These results indicate that mPAO products prepared from single α-olefin monomers exhibit superior mechanical shear resistance compared with those prepared from copolymerized α-olefin systems. This difference may be related to their more uniform molecular structures and more regular chain compositions. As shown in Figure 1b, further analysis of the variation trends within different systems revealed that the viscosity reduction rate exhibited a non-monotonic trend, increasing initially and then decreasing, for both single α-olefin and copolymer systems. For mPAO prepared from single α-olefin monomers, the viscosity reduction rate gradually increased as the carbon number of the original monomer increased from C6 to C10. When the carbon number further increased to C12, the viscosity reduction rate showed a decreasing trend. In comparison, the variation within the copolymer systems was more pronounced. With increasing average carbon number of the monomers, the degree of shear degradation first increased, reached a maximum at C9, and then decreased at C11.

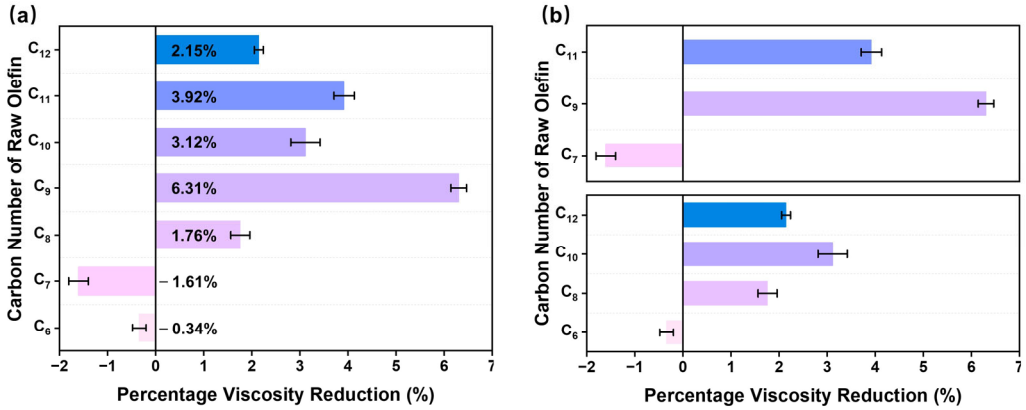


Figure 1. (**a**) Viscosity loss of mPAO prepared from α-olefin monomers with different carbon numbers; (**b**) viscosity loss of mPAO synthesized via different polymerization modes.

Figure 2 shows the changes in molecular weight and molecular weight distribution of different mPAO samples before and after KRL shear testing. Since Mw values exhibit different sensitivities to different regions of the molecular weight distribution, the differences in their changes can be used to analyze the evolution of molecular weight distribution during the shear process. Overall, all samples exhibited a decrease in number-average

molecular weight (Mn) after shear, whereas the changes in weight-average molecular weight (Mw) were relatively small. Meanwhile, the polydispersity index (PDI) generally increased. These results indicate that the KRL shear process does not cause uniform degradation of all molecular chains. Instead, it preferentially affects specific shear-sensitive chain segments [23,24]. Under mechanical shear, polymer chains with higher hydrodynamic resistance and stronger chain-stretching tendency experience greater mechanical stress and are more prone to chain scission. However, the chain fragments generated after scission still retain certain lengths. Therefore, their influence on the overall Mw is weaker than that on Mn. Meanwhile, the newly generated low- and medium-molecular-weight fragments increase the number of molecular chains, causing the molecular weight distribution to gradually extend toward lower molecular weights, ultimately resulting in an increase in PDI. Specifically, the Mn values of the C6 and C7 samples decreased by 3.18% and 0.10%, respectively, whereas their Mw values changed by only +0.40% and +0.12%, respectively. Correspondingly, their PDI values increased by 3.68% and 0.50%, respectively. Notably, the Mw values of the C6 and C7 samples even showed slight increases after shear. However, the changes were both below 0.5%, indicating that no significant high-molecular-weight chain scission occurred during the KRL shear process. Overall, the Mn, Mw, and PDI values of the low-carbon-number samples remained relatively stable before and after shear, suggesting that their molecular weight structures were less affected by mechanical shear.

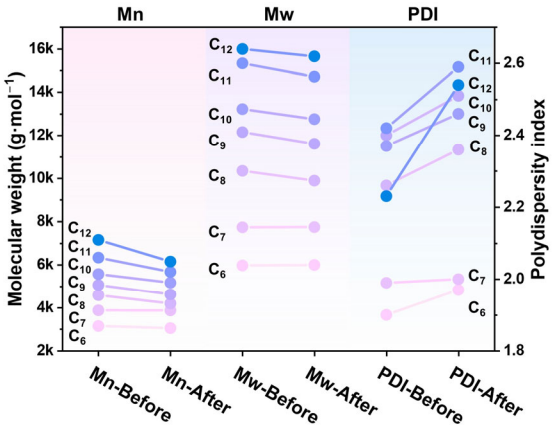


Figure 2. Changes in molecular weight of mPAO before and after shear testing.

With increasing carbon number of the original α-olefin feedstock, the changes in molecular weight distribution induced by shear became increasingly pronounced. The Mn values of the C8, C9, C10, C11, and C12 samples decreased by 8.43%, 8.69%, 7.20%, 10.43%, and 14.09%, respectively, which were significantly higher than those of the C6 and C7 samples. Their PDI values increased by 3.98%, 4.58%, 3.80%, 7.02%, and 13.90%, respectively, indicating that the increase in low-molecular-weight components and the broadening of molecular weight distribution became progressively more significant. Meanwhile, the Mw values of C8, C9, C10, C11, and C12 decreased by 4.45%, 4.50%, 3.52%, 4.05%, and 2.12%, respectively. These changes were smaller than the corresponding decreases in Mn. In particular, although the C11 and C12 samples exhibited relatively large decreases in Mn and increases in PDI, their Mw values decreased by only 4.05% and 2.12%, respectively. This indicates that the shear process mainly involved partial chain scission and an increase in low-molecular-weight components, rather than extensive destruction of the entire high-molecular-weight backbone. In addition, with increasing carbon number of the α-olefin feedstock, changes in side-chain length may influence the stress transfer behavior during mechanical shear [19,25]. For mPAO with shorter side chains, the chain

stretching induced by external mechanical forces is more likely to concentrate on the polymer backbone region, thereby increasing the probability of C-C bond cleavage in the main chain. As the carbon number of α-olefin monomers increases, the alkyl side chains become longer, providing more rotatable C-C bonds and more diverse local conformational states. This enhances the mobility of side chains and chain segments. During mechanical shear, the higher conformational flexibility enables molecular chains to respond to external mechanical perturbations through local conformational adjustments and chain relaxation. This reduces local stress concentration induced by shear and decreases the probability of severe backbone scission in mPAO. However, this proposed mechanism remains hypothetical and requires further validation through molecular simulations or direct experimental evidence.

The FT-IR results shown in Figure 3 further demonstrate that, after KRL shear testing, all samples exhibited new characteristic absorption bands in the wavenumber ranges of 3575–3525 cm^{-1} and 1700–1730 cm^{-1}, corresponding to hydroxyl and carbonyl groups, respectively. These absorption bands were not observed in the spectra of the samples before shearing. These results suggest that, in addition to mechanical shear, oxidation reactions occurred to some extent during the KRL test. As shown in Figure 4, the viscosity, GPC, and FT-IR results suggest that mechanical action may generate highly reactive chain segments or radicals. These species can further react with oxygen in the air, forming oxidation products containing carbonyl groups. The resulting oxygen-containing groups increase molecular polarity and may promote intermolecular association through dipole interactions or hydrogen bonding. This increases flow resistance and leads to a certain degree of oxidative thickening [8,26–28].

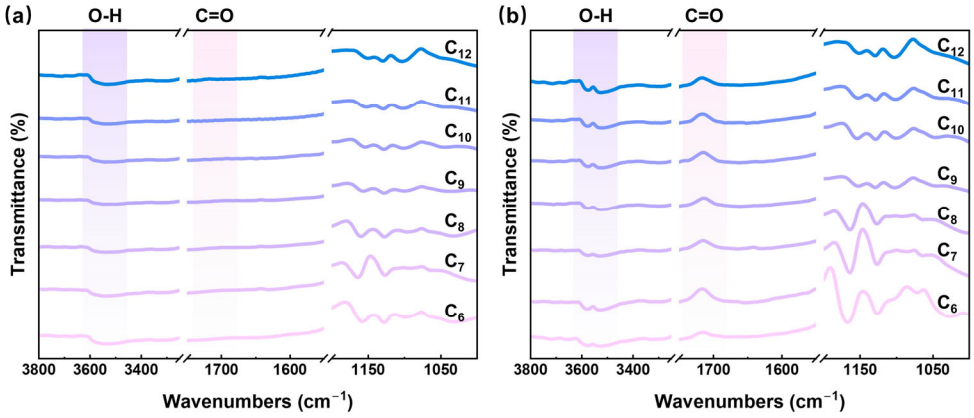


Figure 3. Enlarged regions of the FT-IR of mPAO base oil before and after shear testing: (**a**) before shearing; (**b**) after shearing. The spectra show details in the wavenumber ranges of 3800–3250, 1750–1550, and 1200–1000 cm^{-1}.

Based on the relationship between molecular structure and mechanical shear stability, we propose the following explanation: The C6 and C7 samples showed almost no change in Mw after shearing, with variation rates of only +0.40% and +0.12%, respectively. The changes in Mn and PDI were also small, indicating limited mechanical chain scission. Due to their shorter side chains and lower steric hindrance, the polar groups formed by oxidation in these samples can more easily approach each other and undergo intermolecular association. Therefore, under conditions of relatively weak mechanical degradation, the thickening effect caused by oxidative association may offset or even slightly exceed the viscosity reduction caused by chain scission, resulting in a slight increase in viscosity for the C6 and C7 samples. With a further increase in the carbon number of the original α-olefin feedstock, the side-chain length gradually increases, resulting in enhanced steric

hindrance around the molecular periphery. Longer side chains hinder the effective approach of polar groups formed during oxidation, making intermolecular association more difficult. Therefore, the oxidative thickening effect gradually weakens. Meanwhile, the C9 and C10 samples exhibited more pronounced decreases in both Mn and Mw, accompanied by increases in PDI, indicating that mechanical chain scission became progressively enhanced. Therefore, within the medium carbon-number range, mechanical viscosity reduction gradually became dominant, leading to an increase in the viscosity reduction rate. When the carbon number further increased to C11 and C12, although these samples exhibited the most significant decreases in Mn and increases in PDI, their Mw values decreased by 4.06% and 2.12%, respectively. Among them, the decrease in Mw of the C11 sample was lower than that of the C9 sample in the copolymer system, while the decrease in Mw of the C12 sample was lower than that of the C10 sample in the homopolymer system. This indicates that the changes in molecular weight distribution mainly involved an increase in low-molecular-weight components, while the loss of the high-molecular-weight fraction was relatively limited. Therefore, although oxidative association was further suppressed by the steric hindrance introduced by longer side chains, the preservation of the high-molecular-weight fraction resulted in a reduction in the overall viscosity loss.

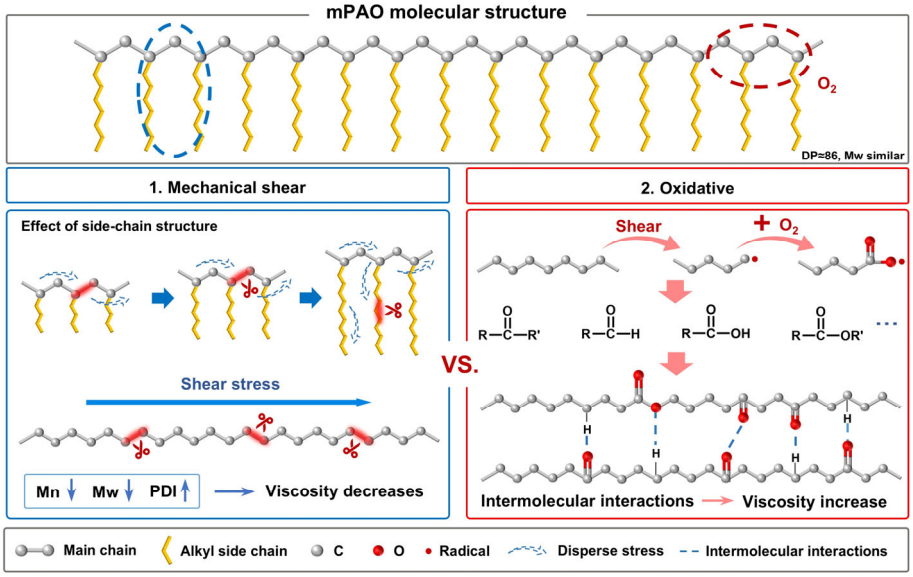


Figure 4. Schematic illustration of the proposed molecular mechanisms governing the mechanical shear response of side-chain mPAO.

Overall, the viscosity reduction rate of mPAO first increased and then decreased with increasing carbon number of the original α-olefin feedstock. This trend results from the competition between two effects: viscosity reduction caused by mechanical chain scission and viscosity increase caused by oxidative association. For samples with lower carbon numbers, shorter side chains and weaker steric hindrance make oxidative association more likely. As a result, the C6 and C7 samples showed slight increases in viscosity. As the side-chain length increased, stronger steric hindrance gradually limited oxidative association. Meanwhile, mechanical chain scission became the dominant effect, leading to a higher viscosity reduction rate. However, at higher carbon numbers, the smaller loss of high-molecular-weight components led to a lower viscosity reduction rate.

3.2. Kinematic Viscosity

To further distinguish the effects of backbone and side-chain structures on shear behavior, the same C8 α-olefin was selected as the polymerization feedstock. This ensured that the side-chain length and chemical structure of all samples remained essentially consistent. Different mPAO samples with various kinematic viscosity grades were obtained by adjusting the degree of polymerization. Therefore, the main structural differences among these samples originated from variations in backbone length and molecular weight. This sample series was used to analyze the effect of backbone growth on the intrinsic mechanical shear stability under fixed side-chain structures.

Figure 5 shows the viscosity reduction rates of mPAO samples with different initial kinematic viscosities after KRL shear testing. Based on the GPC results, the weight-average degree of polymerization (DPw) of each sample was estimated from its weight-average molecular weight (Mw). The relative changes in DPw among different samples were compared to further investigate the effect of polymer backbone length on mechanical shear stability. As the initial kinematic viscosity (at 100 °C) increased from 150 to 400 $mm^2 \cdot s^{-1}$, the DPw of mPAO gradually increased from 64 to 108. Meanwhile, the viscosity reduction rate generally increased from 0.01% to 3.58%. This indicates that increasing backbone length and molecular weight enhanced the sensitivity of mPAO to mechanical shear, resulting in decreased shear stability. It is worth noting that this variation did not exhibit a simple linear increase but showed obvious stage-dependent characteristics. In the range of 150–200 $mm^2 \cdot s^{-1}$, the viscosity reduction rate increased only from 0.01% to 0.59%, remaining at a relatively low level. When the kinematic viscosity increased to 250 $mm^2 \cdot s^{-1}$, corresponding to a DPw of approximately 83, the viscosity reduction rate rapidly increased to 1.69%, showing the first significant increase. Subsequently, within the range of 250–350 $mm^2 \cdot s^{-1}$, the viscosity reduction rate increased slowly from 1.69% to 1.97%. When the kinematic viscosity further increased to 400 $mm^2 \cdot s^{-1}$, corresponding to a DPw of approximately 108, the viscosity reduction rate increased significantly to 3.58%, showing a second and more pronounced increase. Because the side-chain structures of these samples were essentially identical, the above variations mainly reflect the influence of backbone length on mechanical shear behavior. Shorter backbones can better maintain molecular structural integrity under KRL cyclic loading. However, with increasing backbone length, high-molecular-weight chain segments exhibit enhanced ability to bear and transfer mechanical stress, while the probability of chain scission also increases. When the backbone length reaches a certain range, the system transitions from a relatively stable state to a more shear-sensitive region, resulting in a stepwise increase in the viscosity reduction rate. In particular, the sample with a kinematic viscosity of 400 $mm^2 \cdot s^{-1}$ exhibited greater sensitivity to mechanical loading due to its longer backbone, leading to the highest viscosity loss and the lowest mechanical shear stability. Overall, under conditions where the side-chain length remains nearly unchanged, backbone growth significantly increases the mechanical shear sensitivity of mPAO. The viscosity reduction rate increases stepwise with increasing initial kinematic viscosity, with pronounced increases occurring in the ranges of 200–250 $mm^2 \cdot s^{-1}$ and 350–400 $mm^2 \cdot s^{-1}$. These results indicate that the effect of backbone length on mechanical shear stability exhibits a threshold characteristic.

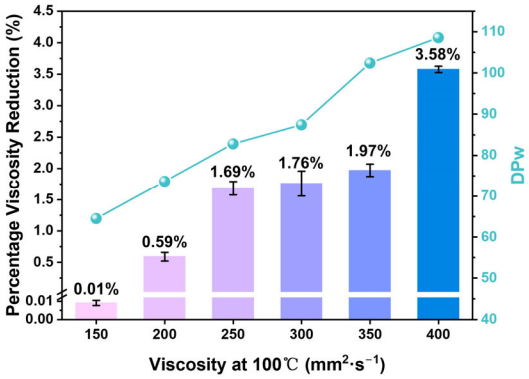


Figure 5. Viscosity loss of mPAO with different initial kinematic viscosities after KRL shear testing.

3.3. Molecular Weight Distribution

Molecular weight distribution is one of the important structural parameters affecting the mechanical response behavior of polymer materials. To further clarify the influence of molecular weight distribution on the mechanical shear stability of mPAO, samples with different PDI values were selected for KRL shear testing, and the variation in kinematic viscosity was analyzed. As shown in Figure 6, the viscosity reduction rate of mPAO samples gradually increased with increasing initial PDI. When the PDI was relatively low, the mPAO-D1 sample exhibited good shear stability, with only a small change in viscosity after shear and a viscosity reduction rate of 1.76%. With further increasing PDI, the viscosity reduction rate gradually increased and reached 5.37% for the mPAO-D5 sample.

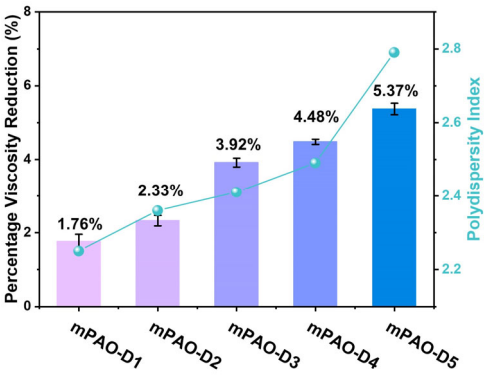


Figure 6. Effect of molecular weight distribution on the mechanical shear stability of mPAO.

These results indicate that a broader molecular weight distribution reduces the mechanical shear stability of mPAO systems, making them more susceptible to viscosity degradation under mechanical loading. From a molecular structure perspective, a higher PDI indicates the presence of more chain segments with different molecular weights within the system, resulting in larger differences in molecular chain length. During cyclic mechanical shear, molecular chains with different lengths exhibit different stress responses. Longer chain segments are more susceptible to stretching and chain scission, while the low-molecular-weight chains generated after scission further broaden the molecular weight distribution and increase structural heterogeneity. Therefore, a broader molecular weight distribution may increase molecular chain instability during shear, accelerate the loss of high-molecular-weight components, and ultimately lead to greater viscosity reduction. Combined with the aforementioned GPC results, the sheared samples generally exhibited decreased Mn values and increased PDI values after KRL shear, indicating that mechanical shear itself induces further broadening of the molecular weight distribution. Therefore, mPAO systems with higher initial PDI values, due to their larger differences in

molecular chain lengths, are more likely to experience structural imbalance during shear and exhibit lower mechanical shear stability.

3.4. Molecular Structural Regularity

In addition to molecular weight and molecular weight distribution, the stereoregularity of polymer chain segments is also an important structural factor affecting mechanical shear response. To investigate the effect of chain stereoregularity on the shear stability of mPAO, four mPAO samples with different stereoregularities were selected for comparative analysis. The samples synthesized using rac-$Me_2Si(ind)_2ZrCl_2$, rac-Me_2Si(4,7-dimethyl-ind)$_2ZrCl_2$, rac-Et(Ind)$_2ZrCl_2$, and meso-Et(Ind)$_2ZrCl_2$ were designated as mPAO-I1, mPAO-I2, mPAO-I3, and mPAO-I4, respectively. The stereosequence distributions were characterized by 13C NMR spectroscopy. As shown in Figure 7b, the resonance signals in the range of 35.50–33.71 ppm can be divided into three regions according to the triad sequences. The region of 35.50–34.96 ppm corresponds to the isotactic mm sequence, 34.96–34.40 ppm corresponds to the heterotactic mr sequence, and 34.40–33.71 ppm corresponds to the syndiotactic rr sequence. The mPAO-I1 exhibited a pronounced dominant peak in the mm region, whereas the signals in the mr and rr regions were relatively weak, indicating a higher proportion of isotactic sequences and a more regular chain configuration. In contrast, the normalized integral fraction of the mm region progressively decreased from mPAO-I2 to mPAO-I4, suggesting a broader distribution of stereosequences and greater configurational randomness along the polymer chains. The KRL shear test results revealed that mPAO-I1 exhibited a viscosity loss of only 1.96%, whereas mPAO-I4 showed a substantially higher viscosity loss of 7.35%. This difference suggests that higher stereoregularity is beneficial to the mechanical shear stability of mPAO, while polymer chains with greater configurational randomness are more susceptible to viscosity reduction under repeated mechanical loading. From a molecular structural perspective, the higher proportion of mm sequences in mPAO-I1 leads to a more regular spatial arrangement of adjacent side chains, which may favor relatively stable and uniform chain conformations, thereby reducing local structural heterogeneity under mechanical loading. In contrast, the higher proportions of mr and rr sequences in mPAO-I4 result in a less ordered spatial distribution of side chains along the polymer backbone. Such configurational irregularity may increase variations in chain conformation and local stress distribution, potentially enhancing the susceptibility of certain chain segments to mechanical shear. Consequently, mPAO-I4 exhibits a greater viscosity loss after the KRL shear test. Combining the 13C NMR and KRL shear results, it can be concluded that a higher content of mm sequences and more regular side-chain arrangements are beneficial for improving the mechanical shear stability of mPAO. In contrast, increased mr and rr sequence contents enhance the heterogeneity of chain conformations, making the samples more sensitive to mechanical shear.

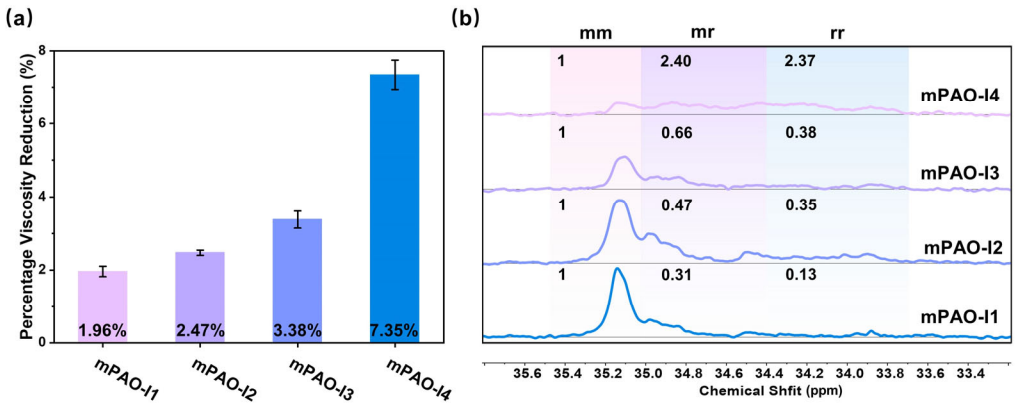


Figure 7. Effect of stereoregularity on the mechanical shear stability and structural characterization of mPAOs: (**a**) viscosity loss of mPAO with different stereoregularities after shear testing; (**b**) ^{13}C NMR spectra of mPAO with different stereoregularities.

3.5. Unsaturated Double-Bond Content

In addition to molecular structural parameters, unsaturated structures in polymer chains are also important factors affecting the mechanical shear stability of mPAO. To investigate the effect of unsaturated double-bond content on shear behavior, mPAO samples with different hydrogenation degrees (mPAO-H1–mPAO-H4) were prepared by adjusting the hydrogenation level. The olefin structures in the molecular chains were characterized by ^{1}H NMR spectroscopy. As shown in Figure 8b, a characteristic signal corresponding to olefinic hydrogen in the R–CH=CH–R structure appeared at 5.0-5.5 ppm in the ^{1}H NMR spectra. To compare the unsaturated double-bond contents of samples with different hydrogenation degrees, the olefinic hydrogen signals were normalized. The relative integral changes in the aliphatic hydrogen region (–CHx) were used to reflect the proportion of unsaturated structures in the molecular chains. With increasing hydrogenation degree, the integral value of the –CHx region increased from 16,625 for mPAO-H1 to 33,644 for mPAO-H4. This indicates that the proportion of saturated alkyl structures in the molecular chains gradually increased, while the unsaturated double-bond content correspondingly decreased.

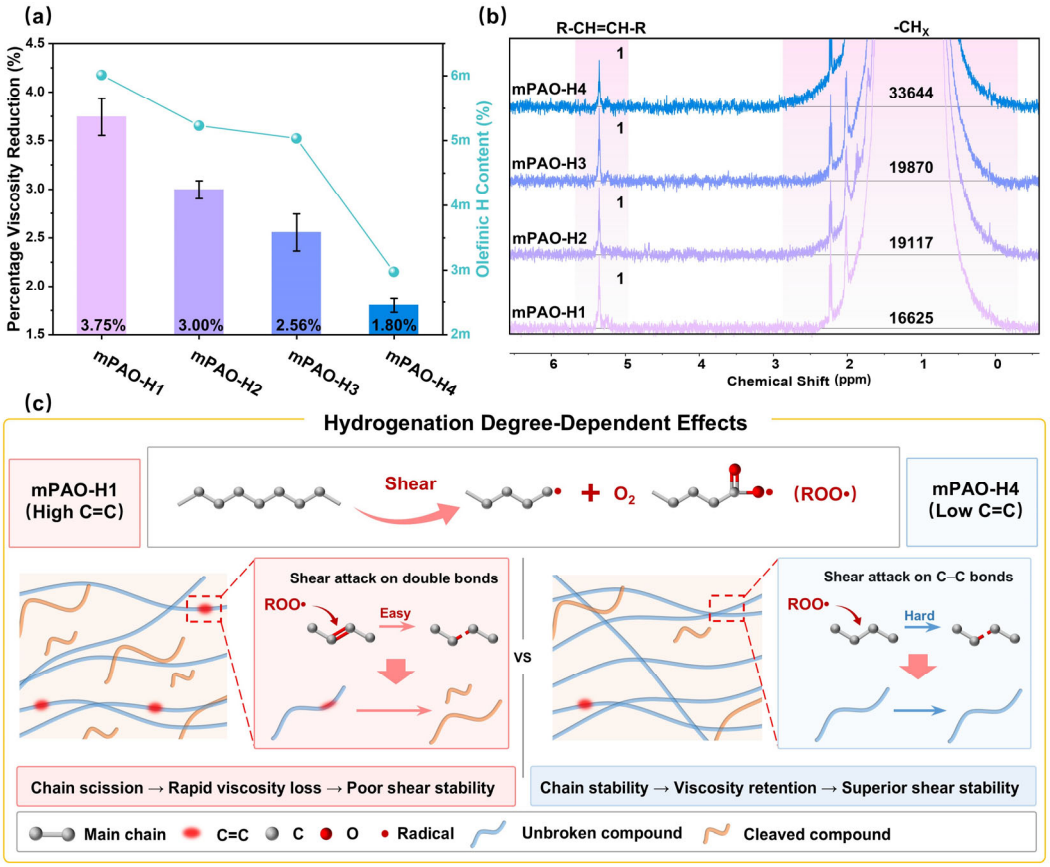


Figure 8. Effect of residual unsaturated structures on the mechanical shear stability and underlying mechanism of mPAO: (**a**) viscosity loss of mPAO with different hydrogenation degrees; (**b**) ^{1}H NMR spectra of mPAO with different hydrogenation degrees; (**c**) schematic illustration of the mechanism by which residual double bonds affect the mechanical shear stability of mPAO.

As shown in Figure 8a, further comparison of viscosity changes in samples with different hydrogenation degrees after KRL shear revealed that the viscosity reduction rate

gradually decreased with decreasing unsaturated double-bond content. Specifically, mPAO-H1 exhibited the highest viscosity reduction rate of 3.75%. With increasing hydrogenation degree, this value decreased successively to 3.00%, 2.56%, and 1.80%, showing a decreasing trend. These results indicate that reducing the unsaturated double-bond content in molecular chains can effectively improve the viscosity retention capability of mPAO under high-shear conditions. This phenomenon is mainly related to the influence of unsaturated double bonds on the chemical stability of molecular chains. As shown in Figure 8c, during the KRL shear process, high shear stress acts on mPAO molecular chains, causing chain stretching and inducing a certain degree of mechanical chain scission. Meanwhile, the high-temperature shear environment promotes the generation of radicals. The C=C double bonds in molecular chains, due to their high reactivity, can act as active sites for oxidation reactions and participate in radical oxidation processes. This leads to the formation of peroxy radicals (ROO•) and oxygen-containing intermediates, thereby accelerating molecular chain degradation and ultimately increasing viscosity loss. Therefore, mPAO samples with higher residual double-bond contents exhibit higher shear sensitivity and more pronounced viscosity degradation during mechanical shear.

In summary, the unsaturated double-bond content is one of the key structural factors determining the intrinsic mechanical shear stability of high-viscosity mPAO. Increasing the hydrogenation degree to reduce the proportion of unsaturated structures in molecular chains can effectively improve the shear resistance of mPAO.

4. Conclusions

This study systematically investigated the effects of molecular structural factors on the shear stability of high-viscosity metallocene poly(α-olefins) under mechanical shear-induced permanent viscosity loss conditions.

Molecular chain topology affects the structural response behavior of mPAO during the shear process. With changes in the carbon number of α-olefin polymerization feedstocks, low-carbon-number samples exhibited limited mechanical chain scission. The polar structures generated by oxidation may undergo intermolecular interactions, thereby compensating for the viscosity reduction effect. As the side-chain length increased, chain scission became more pronounced, while steric hindrance increased and the thickening effect associated with oxidation weakened. These changes led to higher viscosity loss rates. For samples with longer side chains, side-chain motion may help dissipate mechanical stress. This may improve the retention of high-molecular-weight chains and reduce viscosity loss. Under similar side-chain structures, increasing backbone length enhanced shear sensitivity, with viscosity loss showing a threshold-dependent increase. The structural order of molecular chains plays an important role in shear stability. The molecular weight distribution results indicate that a broader molecular weight distribution is unfavorable for maintaining structural stability during shear. In addition, mPAO with a higher proportion of ordered structures exhibited lower viscosity reduction rates, indicating that chain arrangement affects the ability of molecular structures to maintain stability under shear. Unsaturated double-bond content regulates the shear behavior of mPAO by affecting the chemical stability of molecular chains. With decreasing unsaturated double-bond content in mPAO molecular chains, the samples exhibited lower viscosity reduction rates and higher mechanical shear stability. This indicates that unsaturated structures in molecular chains may influence shear-induced chemical reactions, thereby causing significant viscosity changes.

In summary, the mechanical shear stability of high-viscosity mPAO can be directionally optimized by regulating side-chain topology, backbone length, molecular weight distribution, chain stereoregularity, and unsaturated structures. This study establishes the relationship between molecular structure design and shear resistance of high-viscosity

mPAO, providing theoretical guidance for the development of new base oil materials suitable for high-load and long-life lubrication applications.

Supplementary Materials: The following supporting information can be downloaded at https://www.mdpi.com/article/10.3390/lubricants14110436/s1, Scheme S1: Synthetic scheme of 1,2-bis(inden-3-yl)ethane; Figure S1: ^{1}H NMR spectrum of 1,2-bis(inden-3-yl)ethane; Scheme S2: Synthetic scheme of rac-Et(Ind)$_2$ZrCl$_2$ and meso-Et(Ind)$_2$ZrCl$_2$; Figure S2: ^{1}H NMR spectrum of rac-Et(Ind)$_2$ZrCl$_2$ catalyst; Figure S3: ^{1}H NMR spectrum of meso-Et(Ind)$_2$ZrCl$_2$ catalyst; Scheme S3: Synthetic scheme of Dimethylbis(indenyl)silane; Scheme S4: Synthetic scheme of rac-Me$_2$Si(ind)$_2$ZrCl$_2$; Figure S4: ^{1}H NMR spectrum of rac-Me$_2$Si(ind)$_2$ZrCl$_2$ catalyst; Scheme S5: Synthetic scheme of Dimethylbis(4,7-dimethylindenyl)silane; Scheme S6: Synthetic scheme of rac-Me$_2$Si(4,7-dimethyl-ind)$_2$ZrCl$_2$; Figure S5: ^{1}H NMR spectrum of rac-Me$_2$Si(4,7-dimethyl-ind)$_2$ZrCl$_2$ catalyst; Table S1: Changes in kinematic viscosity at 100 °C and viscosity loss of mPAO samples before and after shear testing; Table S2: Changes in molecular weight and molecular weight distribution of mPAO samples before and after shear testing; Table S3: Changes in the degree of polymerization of mPAO prepared from α-olefin monomers with different carbon numbers; Table S4: Changes in kinematic viscosity at 100 °C and viscosity loss of mPAO samples before and after shear testing; Table S5: Molecular weight of mPAO samples; Table S6: Changes in kinematic viscosity at 100 °C and viscosity loss of mPAO samples before and after shear testing; Table S7: Changes in kinematic viscosity at 100 °C and viscosity loss of mPAO samples before and after shear testing; Table S8: Changes in kinematic viscosity at 100 °C and viscosity loss of mPAO samples before and after shear testing; Table S9: Changes in kinematic viscosity at 100 °C and viscosity loss of mPAO samples before and after shear testing.

Author Contributions: Data Curation, Formal Analysis, Investigation, Validation, Visualization, Writing—Original Draft, J.Z.; Funding Acquisition, Project Administration, Resources, Supervision, Writing—Review and Editing, J.X.; Formal Analysis, Z.B.; Formal Analysis, X.L.; Formal Analysis, R.L.; Resources, Supervision, J.S.; Funding Acquisition, Project Administration, Resources, Supervision, Writing—Review and Editing, J.L. All authors have read and agreed to the published version of the manuscript.

Funding: The authors would like to acknowledge financial support for this work from "National Energy Group Ningxia Coal Industry Co., Ltd." (Project No. 20250802NDKJ060).

Data Availability Statement: The data presented in this study are available from the corresponding author upon reasonable request.

Conflicts of Interest: Authors Zhongxiang Bai, Xuemei Liang, Ruilong Li, Jianxin Shi were employed by the company Ningxia Coal Industry Co., Ltd. The remaining authors declare that this research was conducted in the absence of any commercial or financial relationships that could be construed as a potential conflict of interest.

Abbreviations

The following abbreviations are used in this manuscript:

mPAO	metallocene poly(α-olefins)
PVL	permanent viscosity loss
GPC	gel permeation chromatography
FT-IR	Fourier transform infrared spectroscopy

References

1. González, M.O.A.; Jones, D.; Santiso, A.M.; Akbari, N.; Melo, D.C.; Nogueira, L.P.; Vasconcelos, R.M. Offshore Wind and Energy Transition: Lessons Learned, Progress, and Trends. *Annu. Rev. Environ. Resour.* **2025**, *50*, 409–432. https://doi.org/10.1146/annurev-environ-111523-102149.

2. Wojtaszek, H.; Borowski, P.F.; Handschke, M.; Miciuła, I.; Stecyk, A.; Bielawa, A.; Ozdyk, S.; Kowalczyk, A.; Czepło, F. Wind Energy in Transition: Development, Socio-Economic Impacts, and Policy Challenges in Europe. *Energies* **2025**, *18*, 2811. https://doi.org/10.3390/en18112811.
3. Peng, H.; Zhang, H.; Shangguan, L.; Fan, Y. Review of Tribological Failure Analysis and Lubrication Technology Research of Wind Power Bearings. *Polymers* **2022**, *14*, 3041. https://doi.org/10.3390/polym14153041.
4. Bruce, T.; Long, H.; Dwyer-Joyce, R.S. Dynamic modelling of wind turbine gearbox bearing loading during transient events. *IET Renew. Power Gener.* **2015**, *9*, 821–830. https://doi.org/10.1049/iet-rpg.2014.0194.
5. Liu, H.; Liu, H.; Zhu, C.; Sun, Z.; Bai, H. Study on contact fatigue of a wind turbine gear pair considering surface roughness. *Friction* **2019**, *8*, 553–567. https://doi.org/10.1007/s40544-019-0277-3.
6. Ge, G.; Wu, Y.; He, Z.; Wang, S.; van der Heide, E. High-Performance Polymer Composites for Tribological Applications: Matrix Design, Filler Engineering, and Wear Mechanisms. *Polym. Eng. Sci.* **2026**, *66*, 7825–7864. https://doi.org/10.1002/pen.70796.
7. Marx, N.; Ponjavic, A.; Taylor, R.I.; Spikes, H.A. Study of Permanent Shear Thinning of VM Polymer Solutions. *Tribol. Lett.* **2017**, *65*, 106. https://doi.org/10.1007/s11249-017-0888-7.
8. Distler, E.; Albrecht, J.; Holderied, K.; Güney, D.C.; Kiefel, M.; Weber, K. Via Performance to Degradation: Oxidation Mechanism of Biodegradable Polyalphaolefin Base Oil for Electric Drive Systems. *ChemPlusChem* **2025**, *90*, e202500413. https://doi.org/10.1002/cplu.202500413.
9. Liu, M.; Bayer, G.; Reimers, M.; Schünemann, W.; König, F.; Jacobs, G.; Schelenz, R.; Bader, N.; Poll, G.; Marian, M. Towards lifetime lubrication of wind turbine gearboxes: Technical and physical investigations on used oils. *Wear* **2025**, *571*, 205760. https://doi.org/10.1016/j.wear.2025.205760.
10. Fernandes, C.M.C.G.; Marques, P.M.T.; Martins, R.C.; Seabra, J.H.O. Film thickness and traction curves of wind turbine gear oils. *Tribol. Int.* **2015**, *86*, 1–9. https://doi.org/10.1016/j.triboint.2015.01.014.
11. Sharma, B.; Verma, A.; Kukrety, A.; Saini, S.; Kumar, U. Effective polymerization of linear higher alpha olefins from refinery stream for lubricant application. *Polym. Eng. Sci.* **2023**, *63*, 1691–1701. https://doi.org/10.1002/pen.26316.
12. Hu, Q.; Cao, C.; Li, H.; Xu, J.; Han, S.; Li, J. Phosphorus- and sulfur-incorporated chemical modification of metallocene poly-α-olefin for dual-functional base oils with enhanced antioxidant and antiwear performance. *Eur. Polym. J.* **2025**, *240*, 114337. https://doi.org/10.1016/j.eurpolymj.2025.114337.
13. Xue, J.Y.; Dong, S.Q.; Mi, P.K.; Wang, L.B.; Wang, S.H.; Zhang, Z.; Zhang, Z.G.; Hu, J.S. Study of the structure–activity relationship of metallocene-catalysed poly-α-olefin (mPAO) base oil. *Mol. Syst. Des. Eng.* **2021**, *6*, 722–729. https://doi.org/10.1039/d1me00032b.
14. Sparnacci, K.; Frison, T.; Podda, E.; Antonioli, D.; Laus, M.; Notari, M.; Assanelli, G.; Atzeni, M.; Merlini, G.; Pó, R. Core-Cross-linked Star Copolymers as Viscosity Index Improvers for Lubricants. *ACS Appl. Polym. Mater.* **2022**, *4*, 8722–8730. https://doi.org/10.1021/acsapm.2c01039.
15. El-shazly, R.I.; Kamal, R.S.; Farag, R.K. Structural and viscosity studies of dendritic hyper branched polymer as viscosity index improvers. *BMC Chem.* **2024**, *18*, 107. https://doi.org/10.1186/s13065-024-01206-2.
16. Liao, W.; Ju, C.; Zhao, Q.; Lou, W.; Wang, X.; Zhang, S. Synthesis and Properties Study of a Multifunctional Polymethacrylate Viscosity Index Improver. *ACS Appl. Eng. Mater.* **2024**, *3*, 108–117. https://doi.org/10.1021/acsaenm.4c00624.
17. van Ravensteijn, B.G.P.; Bou Zerdan, R.; Seo, D.; Cadirov, N.; Watanabe, T.; Gerbec, J.A.; Hawker, C.J.; Israelachvili, J.N.; Helgeson, M.E. Triple Function Lubricant Additives Based on Organic–Inorganic Hybrid Star Polymers: Friction Reduction, Wear Protection, and Viscosity Modification. *ACS Appl. Mater. Interfaces* **2018**, *11*, 1363–1375. https://doi.org/10.1021/acsami.8b16849.
18. Tian, B.; Shao, Y.; Zhu, F.; Hu, C.; Zhang, T.; Liu, J.; Xu, H.; Cao, C.; Yu, H.; Wang, W. Simulation Study on the Effect of Molecular Structure Characteristics of Lubricant Base Oils on Lubrication Performance. *Lubricants* **2025**, *13*, 398. https://doi.org/10.3390/lubricants13090398.
19. Zhang, J.; Tan, A.; Spikes, H. Effect of Base Oil Structure on Elastohydrodynamic Friction. *Tribol. Lett.* **2016**, *65*, 13. https://doi.org/10.1007/s11249-016-0791-7.
20. Van Sang, L. Simulated Tribological Properties of Pure and Mixed-Base PAO Oils. *Langmuir* **2025**, *41*, 19481–19492. https://doi.org/10.1021/acs.langmuir.5c02218.
21. Wang, W.; Zhang, X.; Li, Y.; Huang, R.; Xu, J.; Yang, L. Effects of molecular structures of poly α-olefin mixture on nano-scale thin film lubrication. *Mater. Today Commun.* **2020**, *25*, 101500. https://doi.org/10.1016/j.mtcomm.2020.101500.
22. Shan, J.; Song, Y.; Wen, P.; Dong, R.; Fan, M. Molecular structure insight into the lubricating performance of heterocyclic ester oil and their film-forming interaction. *Tribol. Int.* **2026**, *214*, 111236. https://doi.org/10.1016/j.triboint.2025.111236.

23. Yu, J.F.S.; Zakin, J.L.; Patterson, G.K. Mechanical degradation of high molecular weight polymers in dilute solution. *J. Appl. Polym. Sci.* **1979**, *23*, 2493–2512. https://doi.org/10.1002/app.1979.070230826.
24. Fujiwara, Y. The superstructure of melt-crystallized polyethylene. I. Screwlike orientation of unit cell in polyethylene spherulites with periodic extinction rings. *J. Appl. Polym. Sci.* **1960**, *4*, 10–15. https://doi.org/10.1002/app.1960.070041002.
25. Farhangi, S.; Weiss, H.; Duhamel, J. Effect of Side-Chain Length on the Polymer Chain Dynamics of Poly(alkyl methacrylate)s in Solution. *Macromolecules* **2013**, *46*, 9738–9747. https://doi.org/10.1021/ma402093v.
26. Blaine, S.; Savage, P.E. Reaction Pathways in Lubricant Degradation. 2. n-Hexadecane Autoxidation. *Ind. Eng. Chem. Res.* **1991**, *30*, 2185–2191. https://doi.org/10.1021/ie00057a020.
27. Blaine, S.; Savage, P.E. Reaction Pathways in Lubricant Degradation. 3. Reaction Model for n-Hexadecane Autoxidation. *Ind. Eng. Chem. Res.* **1992**, *31*, 69–75. https://doi.org/10.1021/ie00001a010.
28. Blaine, S.; Savage, P.E. Reaction Pathways in Lubricant Degradation. 1. Analytical Characterization of n-Hexadecane Autoxidation Products. *Ind. Eng. Chem. Res.* **1991**, *30*, 792–798. https://doi.org/10.1021/ie00052a026.

Disclaimer/Publisher's Note: The statements, opinions and data contained in all publications are solely those of the individual author(s) and contributor(s) and not of MDPI and/or the editor(s). MDPI and/or the editor(s) disclaim responsibility for any injury to people or property resulting from any ideas, methods, instructions or products referred to in the content.